Environmental Science & Technology

Article

pubs.acs.org/est

Transitions from Functionalization to Fragmentation Reactions of Laboratory Secondary Organic Aerosol (SOA) Generated from the OH Oxidation of Alkane Precursors

Andrew T. Lambe,*[,†,‡] Timothy B. Onasch,[†,‡] David R. Croasdale,[†] Justin P. Wright,[†] Alexander T. Martin,[†] Jonathan P. Franklin,[‡] Paola Massoli,[‡] Jesse H. Kroll,[§,∥] Manjula R. Canagaratna,[‡] William H. Brune,[⊥] Douglas R. Worsnop,[‡] and Paul Davidovits[†]

[†]Chemistry Department, Boston College, Chestnut Hill, Massachusetts, United States

[‡]Aerodyne Research, Inc., Billerica, Massachusetts, United States

[§]Department of Civil and Environmental Engineering, Massachusetts Institute of Technology, Cambridge, Massachusetts, United States

[∥]Department of Chemical Engineering, Massachusetts Institute of Technology, Cambridge, Massachusetts, United States

[⊥]Department of Meteorology and Atmospheric Sciences, The Pennsylvania State University, State College, Pennsylvania, United States

Supporting Information

ABSTRACT: Functionalization (oxygen addition) and fragmentation (carbon loss) reactions governing secondary organic aerosol (SOA) formation from the OH oxidation of alkane precursors were studied in a flow reactor in the absence of NO_x. SOA precursors were *n*-decane (*n*-C_{10}), *n*-pentadecane (*n*-C_{15}), *n*-heptadecane (*n*-C_{17}), tricyclo[5.2.1.0^{2,6}]decane (JP-10), and vapors of diesel fuel and Southern Louisiana crude oil. Aerosol mass spectra were measured with a high-resolution time-of-flight aerosol mass spectrometer, from which normalized SOA yields, hydrogen-to-carbon (H/C) and oxygen-to-carbon (O/C) ratios, and $C_xH_y^+$, $C_xH_yO^+$, and $C_xH_yO_2^+$ ion abundances were extracted as a function of OH exposure. Normalized SOA yield curves exhibited an increase followed by a decrease as a function of OH exposure, with maximum yields at O/C ratios ranging from 0.29 to 0.74. The decrease in SOA yield correlates with an increase in oxygen content and decrease in carbon content, consistent with transitions from functionalization to fragmentation. For a subset of alkane precursors (*n*-C_{10}, *n*-C_{15}, and JP-10), maximum SOA yields were estimated to be 0.39, 0.69, and 1.1. In addition, maximum SOA yields correspond with a maximum in the $C_xH_yO^+$ relative abundance. Measured correlations between OH exposure, O/C ratio, and H/C ratio may enable identification of alkane precursor contributions to ambient SOA.

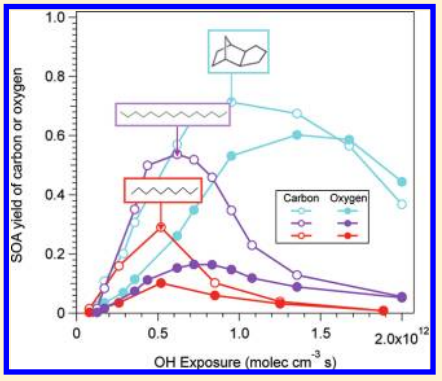

1. INTRODUCTION

Alkanes make up a large fraction of anthropogenic emissions, at times as much as 90%.[1−4] In the atmosphere, alkanes may react with hydroxyl (OH) radicals to form lower-volatility oxidation products that contribute to secondary organic aerosol (SOA). Laboratory studies have identified linear, branched, and cyclic alkanes with carbon numbers ranging from C_7 to C_{25} as possible SOA precursors.[5−8]

The SOA production by oxidation of intermediate volatility and semivolatile alkanes has not been studied extensively[6,8] compared to other biogenic and anthropogenic precursors.[9−11] As a result, intermediate volatility and semivolatile alkanes are typically not included in emissions inventories and chemistry models. However, recent measurements by the National Oceanic and Atmospheric Administration (NOAA) have provided compelling evidence of SOA produced from the atmospheric oxidation of intermediate volatility organic compounds (IVOCs).[12] The NOAA P-3 plane sampled a high-concentration organic aerosol (OA) plume downwind of the offshore Deepwater Horizon (DWH) site during the British Petroleum Gulf oil spill. Gas-phase monitoring instruments in these studies were sensitive to VOCs but not to IVOCs. The spatial distribution of SOA measured downwind of DWH suggested that it was formed from unmeasured IVOC precursors, which were thought to be predominately alkanes.[13] This event represents a unique opportunity to compare ambient and laboratory measurements of SOA generated from alkane precursors.

The present work uses Aerodyne high-resolution time-of-flight aerosol mass spectrometer (HR-ToF-AMS) measurements to examine the chemistry of SOA generated from alkanes

Received: January 23, 2012
Revised: April 14, 2012
Accepted: April 25, 2012
Published: April 25, 2012

over a wide range of OH exposures. SOA was produced from the oxidation of *n*-decane (*n*-C_{10}), *n*-pentadecane (*n*-C_{15}), *n*-heptadecane (*n*-C_{17}), tricyclo[5.2.1.$0^{2,6}$]decane (JP-10), and from vapors of ultra-low-sulfur diesel fuel and Southern Louisiana (SL) crude oil (used as a proxy for oil spilled in the Gulf). One important aspect of this study is the generation of SOA in the absence of NO_x, which can influence the distribution of oxidation products.[14] Another aspect is the use of a flow reactor[15] that can generate OH exposures of up to 2×10^{12} molecules cm^{-3} s, which is approximately ten times higher than exposures attainable using environmental chambers. These higher OH exposures facilitate the characterization of SOA yields and chemical composition over multiple days of equivalent atmospheric oxidation.

2. EXPERIMENTAL SECTION

2.1. SOA Production. SOA particles were generated in a Potential Aerosol Mass (PAM) flow reactor[15,16] by homogeneous nucleation following OH oxidation of gas-phase precursors. The average gas-phase species residence time in the PAM reactor was approximately 100 s. This time scale is long relative to gas-phase oxidation and gas-to-particle transport, but may limit the extent of slower heterogeneous oxidation, oligomerization, and condensed-phase equilibration processes in the reactor.

A carrier gas of 8.5 Lpm N_2 and 0.5 Lpm O_2 was used. A variety of methods were used to introduce gas-phase species into the flow reactor. Decane was prepared in a compressed gas cylinder and introduced at controlled rates using a mass-flow controller. Liquid JP-10 and *n*-C_{15} were evaporated from glass bubblers at controlled rates using a small carrier gas of ultrapure zero air. The *n*-C_{15} bubbler was heated to 45 °C. Other precursors, including *n*-C_{17}, SL crude oil (Onta Inc.), and ultra-low-sulfur diesel fuel (Shell), were introduced into the carrier gas flow using permeation tubes placed in a temperature-controlled oven (T = 30−65 °C) as described by McKinley.[17] A gas chromatograph equipped with a flame ionization detector (GC-FID) was used to characterize the diesel fuel and SL crude oil. These two liquids are composed primarily of C_7 to C_{21} *n*-alkanes together with an unresolved complex mixture of organics that have been identified as predominately branched/cyclic alkanes.[18] The GC-FID method and example chromatograms and volatility distributions of diesel fuel and SL crude oil derived from the chromatograms are discussed in Supporting Information.

2.2. OH Radical Generation. OH radicals were produced via the reaction $O_3 + h\nu \rightarrow O_2 + O(^1D)$ followed by the reaction $O(^1D) + H_2O \rightarrow 2OH$, which is the primary source of atmospheric OH. O_3 was generated by irradiating O_2 with a mercury lamp (λ = 185 nm) outside the PAM reactor. The $O(^1D)$ atoms were produced by UV photolysis of O_3 inside the PAM reactor using four mercury lamps (BHK Inc.), with peak emission intensity at λ = 254 nm. This wavelength enables efficient O_3 photolysis, but may influence yields of species such as organic peroxides that are not affected by atmospheric photolysis at λ > 300 nm. These lamps were mounted in Teflon-coated quartz cylindrical sleeves and were continually purged with N_2. Water vapor was introduced using a heated Nafion membrane humidier (Perma Pure LLC). The humidifier temperature was set to provide a controlled relative humidity in the range of 30−40%.

The OH exposure, which is the product of the OH concentration and the average residence time in the PAM reactor, was obtained indirectly by measuring the decay of SO_2 due to reaction with OH. The OH concentration was varied by changing the UV light intensity through stepping the lamp voltages between 0 and 110 V. SO_2 calibration measurements were conducted as a function of UV lamp intensity and O_3 concentration,[16] and in the presence and absence of alkane precursors to correct for reductions in OH levels following addition of precursors to the flow reactor. This correction ranged from 10% at the highest OH exposure to 50% at the lowest OH exposure. After correction, OH exposures ranged from 8×10^{10} to 2×10^{12} molecules cm^{-3} s. In the absence of NO_x, organic peroxy (RO_2) radicals formed from initial OH oxidation of alkane precursors react with other RO_2 or hydroperoxy (HO_2) radicals. The reduction in OH exposure following precursor addition indicates that RO_2-RO_2 self-reactions may be competitive with RO_2-HO_2 reactions, particularly at high precursor concentrations and low OH exposures.

Exposures in this range are equivalent to 0.6−15 days of atmospheric oxidation assuming an average atmospheric OH concentration of 1.5×10^6 molecules cm^{-3}.[19] Although OH concentrations in these experiments (approximately 8×10^8 to 2×10^{10} molecules cm^{-3}) are higher than ambient OH concentrations, the integrated OH exposures are similar. Previous work suggests that, to first order, extrapolation of flow tube reactor conditions (high [OH], short exposure times) to atmospheric conditions (low [OH], long exposure times) is reasonable.[20]

2.3. Particle Monitoring and Analysis. Particle size distributions were measured with a scanning mobility particle sizer (SMPS, TSI 3080) operated at a 5:1 sheath-to-aerosol flow ratio. Prior to each experiment, the PAM reactor was conditioned with OH radicals until a particle background less than 10 particles cm^{-3} was attained.

2.3.1. SOA Yields. For a subset of precursors (*n*-C_{10}, *n*-C_{15}, and JP-10), it was possible to obtain an approximate measure of the absolute SOA yield using the vapor pressure of the precursor.[21,22] SOA yields were corrected for size-dependent wall losses based on particle transmission measurements of bis(2-ethylhexyl) sebacate.[16] These corrections were approximately a factor of 2 in magnitude. Corrections applied to measured smog chamber SOA yields result in overall uncertainties ranging from 10% to 100%.[23]

2.3.2. SOA Mass Spectra. Aerosol mass spectra were measured with a Aerodyne HR-ToF-AMS that was operated in V-mode[24] and analyzed using ToF-AMS analysis software (Squirrel and Pika),[25] which yielded high-resolution (HR) mass spectra, elemental ratios, and abundances of the $C_xH_y^+$, $C_xH_yO^+$, and $C_xH_yO_2^+$ HR ion groups containing zero, one, and two or more oxygen atoms per ion, respectively. Organic O^+, OH^+, H_2O^+, and CO^+ ions were included in the $C_xH_yO_2^+$ group because these species were calculated from the organic CO_2^+ ion abundance using the recommendations of Aiken et al.[26] The combined $C_xH_y^+$, $C_xH_yO^+$, and $C_xH_yO_2^+$ signals account for >99% of the total organic signal measured by the AMS.

3. RESULTS AND DISCUSSION

3.1. Representative Mass Spectra of SOA Generated from Alkanes. Figure 1a and b show mass spectra of SOA generated from the oxidation of *n*-C_{17} at OH exposures of 8×10^{10} and 2×10^{12} molecules cm^{-3} s, respectively. These spectra illustrate the least- and most-oxidized SOA generated in this work, with corresponding O/C ratios equal to 0.13 and 1.33,

dx.doi.org/10.1021/es300274t | Environ. Sci. Technol. 2012, 46, 5430−5437

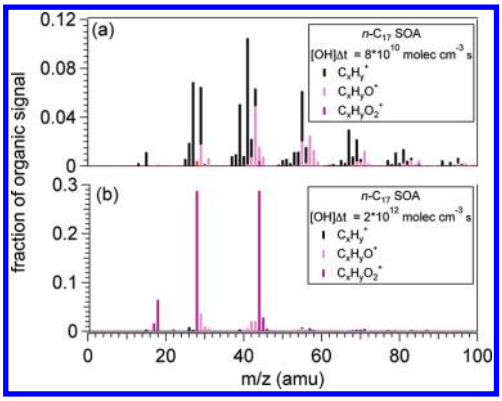

Figure 1. Mass spectra of laboratory SOA generated from n-C_{17} at OH exposures of (a) 8×10^{10} and (b) 2×10^{12} molecules cm^{-3} s. Colors are based on classification in $C_xH_y^+$, $C_xH_yO^+$, and $C_xH_yO_2^+$ organic ion groups.

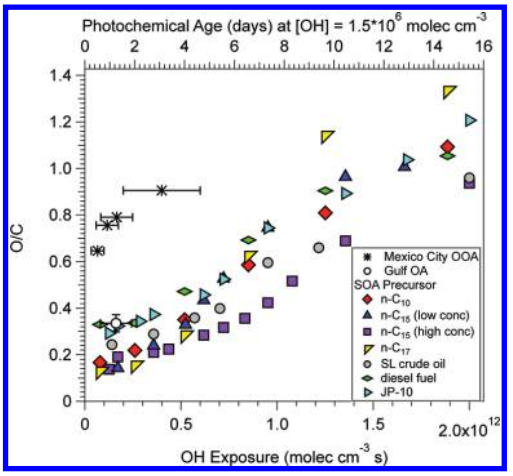

Figure 2. O/C ratio of SOA produced from laboratory alkane precursors and of ambient OA produced downwind of Mexico City and the Gulf oil spill as a function of OH exposure. Mexico City data points correspond to flights over T0, T1 (T0 + 3 h), T2 (T0 + 6 h), and the most-oxidized OA measured during the campaign.[40] Equivalent photochemical age is shown on the top axis assuming an average atmospheric OH concentration of 1.5×10^6 molecules cm^{-3}.

respectively. Mass spectral colors are based on classification in the $C_xH_y^+$, $C_xH_yO^+$, and $C_xH_yO_2^+$ ion groups. These mass spectra span the range of oxidation levels observed in ambient OA ranging from hydrocarbon-like organic aerosol (HOA) to oxygenated organic aerosol (OOA).[27] The mass spectrum shown in Figure 1a has a regularly spaced pattern of alkyl fragments characteristic of unoxidized alkanes (NIST Chemistry Webbook), with additional contributions from oxygenated ions. This spectrum is similar to a reference ambient HOA unit mass resolution (UMR) spectrum[28] with the m/z = 39 ($C_3H_3^+$) signal removed (r^2 = 0.84), as it is present in our spectrum but not in the reference spectrum because of potential interference with potassium (K^+) ions in UMR. Figure 1b shows that the highly oxidized SOA generated from n-C_{17} is dominated by m/z = 44 (CO_2^+), which is a mass spectral fragment of organic acids measured in the AMS.[26] This spectrum is well correlated with a reference ambient OOA spectrum[28] (r^2 = 0.83).

The generation of laboratory SOA that resembles ambient HOA is noteworthy because HOA is often associated with primary organic aerosol (POA).[29−31] Recent studies have demonstrated both the high volatility of POA and the SOA formation potential of IVOC and SVOC alkane precursors present in primary emissions.[32−34] Our results suggest that ambient POA, after evaporation into the gas phase and oxidation by OH, may form ambient SOA resembling HOA. The similarity between the observed laboratory SOA and ambient HOA may also indicate that the HOA factor determined from ambient data sets is a convolution of POA and lightly oxidized SOA.[35]

3.2. OH Exposure and O/C Ratio As Measures of Oxidative Aging. To relate laboratory measurements presented in this paper to ambient measurements, oxidant exposure and the resulting O/C ratio of the SOA can both be used as measures of atmospheric oxidative aging.[36,37] The validity of this correlation is demonstrated in Figure 2, which shows the O/C ratio of laboratory SOA generated from alkane precursors as a function of OH exposure. For each type of SOA, $r^2 \geq 0.95$, suggesting that the two parameters are approximately linearly related.

A primary advantage of SOA O/C is that it is currently measured in both the laboratory and field, whereas OH exposure is typically estimated. Another advantage of using the O/C ratio in place of the oxidant exposure is that other parameters that can influence the oxidation level of the SOA, such as the SOA mass loading, are incorporated into the O/C ratio. Figure 2 shows measurements from two separate experiments in which different concentrations of n-C_{15} were used to produce SOA. At a specific OH exposure, the O/C ratio is higher at lower SOA concentrations, where concentrations range from 1 to 16 μg m^{-3} in one experiment and 2 to 100 μg m^{-3} in the other. This result is consistent with the expected behavior for equilibrium partitioning of semivolatile organic compounds into the condensed phase.[38,39]

To compare the relationship between O/C ratio and OH exposure for laboratory SOA produced from alkanes and ambient OA influenced by anthropogenic precursors, Figure 2 shows measurements for OA sampled downwind of the Gulf oil spill[13] and the Mexico City metropolitan area during the MILAGRO campaign.[40] Calculation of ambient OH exposures from these studies is presented in Supporting Information, including assumptions made regarding average daytime and 24-h OH concentrations.[13,41,42] Figure 2 shows that OH exposures required to produce SOA with O/C ≈ 0.3 from evaporated IVOCs in the Gulf and from SL crude oil vapors in the laboratory agree within a factor of 2. Corresponding aerosol concentrations ranged from 2 to 12 μg m^{-3} for OA produced in the Gulf[12] and from 0.8 to 15 μg m^{-3} for laboratory SOA produced from SL crude oil. On the other hand, OA produced downwind of Mexico City had a higher O/C ratio than SOA formed in the Gulf and in the laboratory at comparable OH exposures. Dzepina et al.[41] modeled the O/C ratio of SOA formed downwind of Mexico City and found that inclusion of IVOC precursors reproduced observed SOA concentrations better, but measured and modeled O/C ratios were in better agreement by assuming SOA was produced from the oxidation of traditional VOC precursors such as aromatics, alkenes, and $<C_{12}$ alkanes (O/C ≈ 0.5−0.6) rather than IVOC precursors (O/C ≈ 0.2−0.4). This discrepancy in O/C ratio is comparable to that observed in the laboratory and field studies shown in Figure 2. Thus, precursor identity, volatility, and other potential factors (e.g., VOC/NO_x ratio) may influence the O/C ratio of SOA at a specific OH exposure.

3.3. Functionalization and Fragmentation Regimes Observed in Alkane SOA Yields. Figure 3 shows the

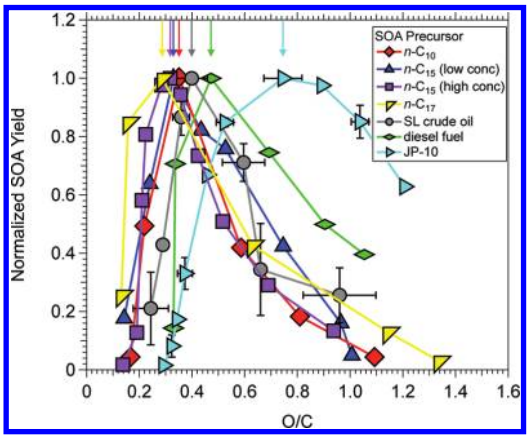

Figure 3. Normalized SOA yields as a function of O/C ratio for laboratory SOA generated from alkanes. For each of the precursors, yields were normalized to the maximum SOA yield. The O/C ratio at maximum yield is indicated by arrow markers. Representative error bars indicate $\pm 1\sigma$ uncertainty in measurements.

normalized yields of SOA generated from n-C_{10}, n-C_{15}, n-C_{17}, SL crude oil, diesel fuel, and JP-10 as a function of O/C ratio. For each of the precursors, yields were normalized to the maximum SOA yield, and the O/C ratio at maximum yield is indicated by an arrow marker. As is evident from Figure 3, the SOA yield increases and then decreases with increasing O/C ratio. A pattern is evident between the O/C ratio at which maximum SOA yields occur and the precursor structure. Maximum yields occur at lower O/C ratio for linear alkanes (O/C = 0.29−0.35), at midrange O/C ratios for mixtures of linear, branched, and cyclic alkanes (SL crude oil and diesel fuel; O/C = 0.40 and 0.47), and at a higher O/C ratio for JP-10, a tricyclic alkane (O/C = 0.74). Similar patterns have been observed in previous studies.[6]

In addition to precursor structure and oxidation level, precursor concentration is another parameter that can affect SOA yields as a result of changing kinetics and/or phase partitioning.[38,39] For one of the precursors (n-C_{15}), experiments were conducted where the initial precursor concentration was increased from approximately 73 to 146 μg m^{-3}. Although the corresponding SOA concentrations (i.e., yields) for a given OH exposure increased by about factor of 5, the O/C ratio at which the maximum SOA yield occurred remained unchanged, as is shown in Figure 3.

As discussed in Section 3.3, it was possible to estimate the absolute SOA yields of n-C_{10}, n-C_{15}, and JP-10 as a function of OH exposure. Maximum SOA yields of 0.39 (n-C_{10}), 0.69 (n-C_{15}), and 1.1 (tricyclo[5.2.1.0^{2,6}]decane) were measured at SOA concentrations of 231, 100, and 306 μg m^{-3}, respectively. Our measurements suggest that the SOA yield increases with carbon number and cyclic structure.[6,8] However, alkane SOA yields are lower at more typical atmospheric mass loadings. For example, the maximum SOA yield of n-C_{15} is 0.21 at an SOA concentration of 16 μg m^{-3}.

To our knowledge, our measurements are the first reported yields for SOA produced from the oxidation of alkanes in the absence of NO_x. SOA yields from the OH oxidation of more widely studied precursors such as α-pinene and toluene range from approximately 0.06 to 0.46 and 0.18 to 0.66 in the absence of NO_x, depending on precursor concentration.[10,11,43] As alkane SOA yields fall in a similar range, more extensive characterization of alkane SOA yields under low-NO_x conditions is planned for future studies.

The trends in SOA yields from Figure 3 reflect a competition among condensation, functionalization, and fragmentation processes. Functionalization reactions at lower OH exposures produce low vapor pressure gas-phase species that readily condense to form SOA. Continued oxidation, however, also results in fragmentation reactions that cleave carbon−carbon bonds and form higher vapor pressure products that result in a lower SOA yield.[44−46] To relate the trends in these different processes to chemical changes in the SOA, Figure 4 shows the

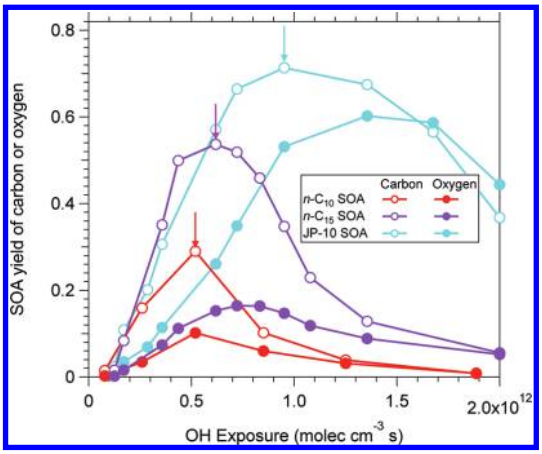

Figure 4. Absolute carbon and oxygen SOA yields as a function of OH exposure for laboratory SOA generated from n-C_{10}, n-C_{15}, and JP-10. Arrows point to OH exposure at maximum SOA yields from Figure 3.

SOA yields of carbon and oxygen (Y_C, Y_O) produced from n-C_{10}, n-C_{15}, and JP-10. Y_C and Y_O were calculated using eqs 1 and 2, which are derived in the Supporting Information:

$$Y_C = \frac{C_{SOA}}{C_{PRE}} \times \frac{12}{12 + 16 \times O/C + H/C} \quad (1)$$

$$Y_O = Y_C \times O/C \quad (2)$$

where C_{SOA} and C_{PRE} are the mass concentrations of SOA and precursor. The maximum Y_C is associated with the maximum SOA yield from Figure 3. The maximum Y_O occurs after the maximum yield for SOA produced from n-C_{15} and JP-10. These results suggest that the maximum SOA yield is controlled at least in part by the transition from functionalization to fragmentation reactions. Functionalization reactions (addition of oxygen-containing functional groups) decrease product volatility, leading to efficient condensation and thus increases in Y_C and Y_O. Fragmentation reactions (breaking of carbon−carbon bonds) increase product volatility and thus decreases in Y_C and Y_O. In general, Y_C decreases more rapidly than Y_O, which may reflect a gradual transition from functionalization to fragmentation.

The relationship between chemical composition and oxidation level is further examined in Figure 5, where fractions of AMS organic signal contained in the $C_xH_y^+$, $C_xH_yO^+$, and $C_xH_yO_2^+$ ion groups are shown as a function of O/C ratio. Figure 5a shows that the $C_xH_y^+$ fraction decreases monotonically. The $C_xH_yO^+$ ion group with intermediate oxygen content (Figure 5b) shows an increase and then decrease, with a

dx.doi.org/10.1021/es300274t | Environ. Sci. Technol. 2012, 46, 5430−5437

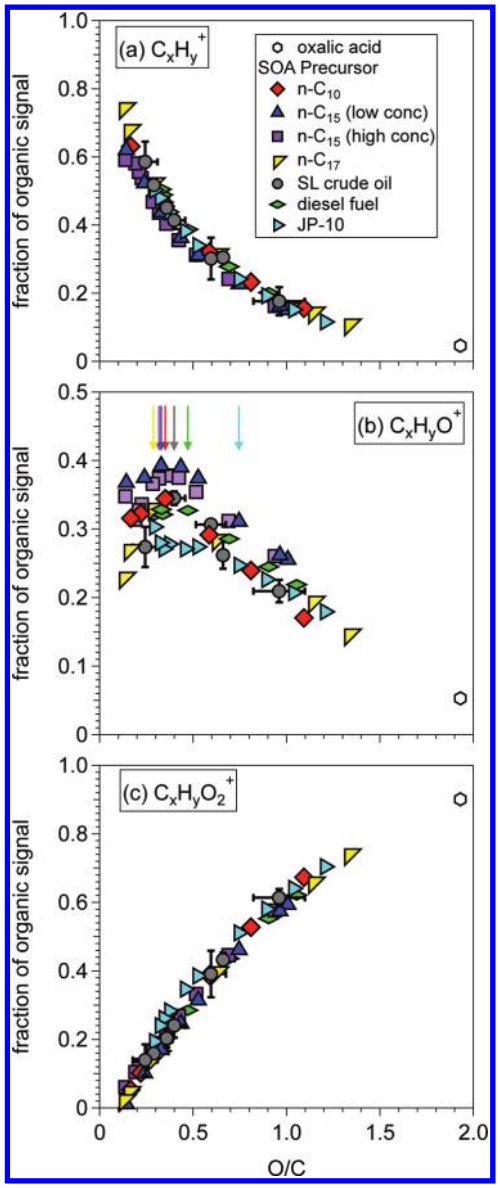

Figure 5. Relative abundance of mass spectral organic (a) $C_xH_y^+$, (b) $C_xH_yO^+$, and (c) $C_xH_yO_2^+$ ion groups as a function of O/C ratio for laboratory SOA generated from alkanes. HR family abundances for oxalic acid are shown for reference. Representative error bars indicate $\pm 1\sigma$ uncertainty in measurements. Arrows point to O/C ratio at maximum SOA yields from Figure 3.

maximum value at the O/C ratio associated with the maximum SOA yield. In the case of SOA produced from JP-10, the $C_xH_yO^+$ fraction is initially constant before decreasing at the O/C ratio associated with the maximum SOA yield. The $C_xH_yO_2^+$ ion group in Figure 5c is characteristic of highly oxidized species such as carboxylic acids; as is evident, its contribution increases monotonically with O/C ratio.

These mass spectral ion group observations are consistent with the reactive loss of hydrocarbon precursors and the formation of RCO and RCO_2 functional groups due to functionalization reactions. At low O/C ratio, Figure 5 indicates that alkane oxidation products nucleate/condense once the fraction of $C_xH_yO^+$ ions exceeds 0.2, whereas the fraction of $C_xH_yO_2^+$ ions is less than 0.05. To first order, $C_xH_yO^+$ ions represent intermediate oxidation products that are converted to $C_xH_yO_2^+$ ions via fragmentation reactions.[44] However, $C_xH_yO_2^+$ ions can in principle also be formed via functionalization reactions. AMS organic signals at m/z = 43 and m/z = 44 are also used as markers for lightly and heavily oxidized OOA.[47] Linear correlation coefficients (r^2) were 0.71 between m/z = 43 and $C_xH_yO^+$, and 0.97 between m/z = 44 and $C_xH_yO_2^+$. Thus, $C_xH_yO^+$ and $C_xH_yO_2^+$ behave similarly to m/z = 43 and m/z = 44. The correlation between $C_xH_yO_2^+$ and m/z = 44 is higher because organic H_2O^+, CO^+, and CO_2^+ ions usually contributed >90% of the $C_xH_yO_2^+$ signal.

Figure 5 also shows the $C_xH_y^+$, $C_xH_yO^+$, and $C_xH_yO_2^+$ fractions for oxalic acid, which represents the most highly oxidized compound that has been measured in organic aerosols.[31,48] Figure 5 shows that the $C_xH_y^+$, $C_xH_yO^+$, and $C_xH_yO_2^+$ fractions of alkane SOA extrapolate to those of oxalic acid. This suggests that oxalic acid may represent a condensed-phase oxidation end point for alkane SOA.

3.4. Van Krevelen Diagrams for Alkane SOA. Van Krevelen diagrams that show H/C ratio as a function of O/C ratio have been used to deduce oxidation reaction mechanisms for organic aerosols.[49] A Van Krevelen diagram obtained from laboratory SOA produced from alkanes is shown in Figure 6. A Van Krevelen diagram comparing the H/C and O/C ratios of laboratory alkane SOA to ambient OA measured downwind of the Gulf oil spill[13] and Mexico City[40] is shown in Figure 7.

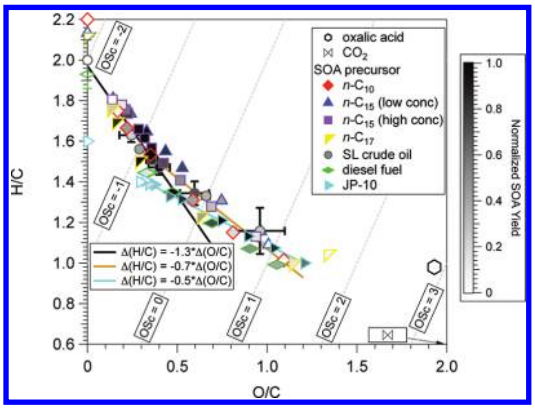

Figure 6. Van Krevelen diagrams showing H/C ratio as a function of O/C ratio for laboratory SOA generated from alkanes. Carbon oxidation state (OSc = 2 × O/C − H/C) isobars and H/C and O/C ratios of oxalic acid (measured) and CO_2 (atomic) are shown for reference. Representative error bars indicate $\pm 1\sigma$ uncertainty in measurements. Lines represent different slopes fit in the data (see text for details). Black fit line has been extended to higher O/C to guide the eye. Gray colorbar shows normalized yield measurements (Figure 3) and shows a correlation between maximum yields and changes in Van Krevelen slope.

3.4.1. Interpreting Changes in Van Krevelen Slope. The Van Krevelen slope, $\Delta(H/C)/\Delta(O/C)$, can provide additional information about functional group formation in the SOA due to oxidative aging. As discussed in Heald et al.,[49] a Van Krevelen slope of zero ($\Delta H/C = 0$) is consistent with addition of alcohol or peroxide functional groups to a carbon backbone, assuming no fragmentation occurs. A slope of −2 ($\Delta H/C = -2 \times \Delta O/C$) is attributed to the addition of aldehyde or ketone functional groups, and a slope of −1 ($\Delta H/C = -\Delta O/C$) is consistent with formation of carboxylic acid functional groups, or alcohol plus aldehyde/ketone groups on different carbon atoms.

dx.doi.org/10.1021/es300274t | Environ. Sci. Technol. 2012, 46, 5430−5437

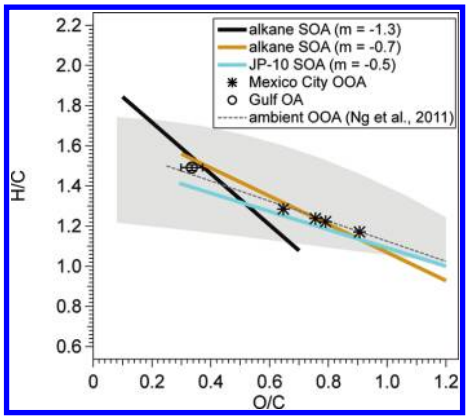

Figure 7. Van Krevelen diagram comparing H/C ratio as a function of O/C ratio for laboratory SOA produced from alkanes (represented by fit lines from Figure 6) to ambient OA produced downwind of Mexico City[40] and the Gulf oil spill.[13] Shaded gray region represents range of H/C and O/C ratios found in ambient OOA.[50].

Figure 6 shows the Van Krevelen diagram for laboratory SOA generated from alkane precursors. Open symbols represent different precursors, and closed symbols representing SOA are shaded by the corresponding normalized SOA yield values (Figure 3). The initial Van Krevelen slope is linear up to O/C ≈ 0.3, with a value of −1.3 ± 0.2. Thereafter, the slope becomes less negative with a value of −0.7 ± 0.1 up to O/C ≈ 1. We also show the AMS-measured H/C and O/C ratios for oxalic acid, and the atomic H/C and O/C ratios for CO_2. The initial change in Van Krevelen slope from −1.3 to −0.7 at O/C ≈ 0.3 correlates with the measured O/C ratio of maximum yield and $C_xH_yO^+$ signal for SOA produced from *n*-alkanes and SL crude oil (Figure 3). These correlated changes are consistent with transitions from functionalization- to fragmentation-dominated reactions. In particular, a less negative Van Krevelen slope can arise from preferential loss of carbon relative to oxygen.[50] Similar changes in Van Krevelen slope have been observed from the heterogeneous oxidation of squalane.[44]

An examination of AMS spectra for alkane SOA shows that at low oxidation levels (e.g., Figure 1a), the SOA contains relatively high levels of $C_xH_yO^+$ ions that are characteristic of carbonyl species. At higher oxidation levels, $C_xH_yO_2^+$ ions dominate the spectrum (Figure 1b). This observation, together with the Van Krevelen slopes, suggest an alkane oxidation mechanism that results in production of carbonyl groups at low oxidation levels with minimal fragmentation, and carboxylic acid groups at high oxidation levels with significant fragmentation.

Changes in Van Krevelen slope were less pronounced for SOA produced from diesel fuel and JP-10, with JP-10 exhibiting the largest differences. Diesel fuel and JP-10 have lower H/C ratios than the other studied precursors, and this appears to influence the oxidative aging mechanism at low oxidant exposures (O/C ratios), specifically in terms of functional groups produced and extent of fragmentation. In addition, the onset of SOA formation from diesel fuel and JP-10 occurs at higher O/C ratios than the other precursors, with corresponding higher relative abundance of $C_xH_yO_2^+$ and yields peaking at higher O/C ratios. The H/C and O/C ratios of SOA produced from JP-10 are characterized by a separate line with a Van Krevelen slope of −0.5. There are several combinations of functional group additions that can produce a slope of −0.5. However, two scenarios that are unique to cyclic precursors such as JP-10 include production of two carboxylic acid groups, or two carbonyl plus two alcohol groups, following ring-opening oxidation by OH.

3.4.2. Implication for Ambient Measurements. Figure 7 shows the Van Krevelen slopes obtained from the laboratory SOA experiments together with ambient data. Ambient OOA components occupy the gray shaded region in Figure 7 and follow an average Van Krevelen slope of about −0.5, which is indicated by the dashed line.[50] Circle and star symbols represent H/C and O/C ratios of OA produced downwind of the Gulf oil spill and Mexico City. Despite different trends between O/C ratio and OH exposure for laboratory SOA and Mexico City OOA, Figure 7 shows that the elemental composition and Van Krevelen slopes are similar. Alkane SOA is additionally distinguished by a steeper Van Krevelen slope for O/C < 0.3 and a sharp transition from functionalization- to fragmentation-dominated reaction mechanisms. This feature, together with the measured correlations between O/C ratio and OH exposure (Figure 2) and trends in $C_xH_y^+$, $C_xH_yO^+$, and $C_xH_yO_2^+$ ion groups as a function of oxidation level (Figure 5), may be useful for identifying ambient SOA that is produced from alkane precursors, especially IVOC alkanes such as those emitted during the Gulf oil spill. At higher OH exposures and oxidation levels (e.g., O/C > 0.3), AMS signatures of alkane SOA are less distinct, to the point that they can no longer be readily distinguished from other species. Measurement techniques facilitating detailed, molecular-level characterization of SOA may be required under these conditions and will be investigated in future work.

■ ASSOCIATED CONTENT

Supporting Information

GC-FID chromatograms and volatility distributions of diesel fuel and SL crude oil, calculations of ambient OH exposures for SOA measured downwind of the Gulf oil spill and Mexico City, SOA yield calculations, and derivations of Y_C and Y_O. This material is available free of charge via the Internet at http://pubs.acs.org.

■ AUTHOR INFORMATION

Corresponding Author

*E-mail: andrew.lambe@bc.edu.

Notes

The authors declare no competing financial interest.

■ ACKNOWLEDGMENTS

We thank Tiffany Samuelson, Kenneth Christian, and Diana van Duin (Pennsylvania State University) for preparing compressed VOC canisters. We thank Leah Williams and Charles Kolb (ARI) for helpful discussions, and Roya Bahreini (NOAA) for supplying Southern Louisiana crude oil. This research was supported by the Office of Science (BER), Department of Energy (Atmospheric Science Program) grants DE-SC0006980 and DE-FG02-05ER63995, and the Atmospheric Chemistry Program of the National Science Foundation grants ATM-0854916 and AGS-0904292 to Boston College and Aerodyne Research, Inc.

■ REFERENCES

(1) Rogge, W. F.; Hildemann, L. M.; Mazurek, M. A.; Cass, G. R.; Simoneit, B. R. T. Sources of fine organic aerosol. 3. Road dust, tire

debris, and organometallic brake lining dust: roads as sources and sinks. *Environ. Sci. Technol.* **1993**, *27*, 1892−1904.
(2) Fraser, M. P.; Cass, G. R.; Simoneit, B. R. T.; Rasmussen, R. A. Air Quality Model Evaluation Data for Organics. 4. C2- C36 Non-Aromatic Hydrocarbons. *Environ. Sci. Technol.* **1997**, *31*, 2356−2367.
(3) Schauer, J. J.; Kleeman, M. J.; Cass, G. R.; Simoneit, B. R. T. Measurement of emissions from air pollution sources. 2. C1 through C30 organic compounds from medium duty diesel trucks. *Environ. Sci. Technol.* **1999**, *33*, 1578−1587.
(4) Schauer, J. J.; Kleeman, M. J.; Cass, G. R.; Simoneit, B. R. T. Measurement of Emissions from Air Pollution Sources. 5. C1- C32 Organic Compounds from Gasoline-Powered Motor Vehicles. *Environ. Sci. Technol.* **2002**, *36*, 1169−1180.
(5) Lim, Y. B.; Ziemann, P. J. Products and mechanism of secondary organic aerosol formation from reactions of n-alkanes with OH radicals in the presence of NO_x. *Environ. Sci. Technol.* **2005**, *39*, 9229−9236.
(6) Lim, Y. B.; Ziemann, P. J. Effects of molecular structure on aerosol yields from OH radical-initiated reactions of linear, branched, and cyclic alkanes in the presence of NO_x. *Environ. Sci. Technol.* **2009**, *43*, 2328−2334.
(7) Presto, A. A.; Miracolo, M. A.; Kroll, J. H.; Worsnop, D. R.; Robinson, A. L.; Donahue, N. M. Intermediate-volatility organic compounds: A potential source of ambient oxidized organic aerosol. *Environ. Sci. Technol.* **2009**, *43*, 4744−4749.
(8) Presto, A. A.; Miracolo, M. A.; Donahue, N. M.; Robinson, A. L. Secondary organic aerosol formation from high-NO_x photo-oxidation of low volatility precursors: n-alkanes. *Environ. Sci. Technol.* **2010**, *44*, 2029−2034.
(9) Ng, N. L.; Kroll, J. H.; Chan, A. W. H.; Chhabra, P. S.; Flagan, R. C.; Seinfeld, J. H. Secondary organic aerosol formation from m-xylene, toluene, and benzene. *Atmos. Chem. Phys.* **2007**, *7*, 3909−3922.
(10) Ng, N. L.; Chhabra, P. S.; Chan, A. W. H.; Surratt, J. D.; Kroll, J. H.; Kwan, A. J.; McCabe, D. C.; Wennberg, P. O.; Sorooshian, A.; Murphy, S. M.; Dalleska, N. F.; Flagan, R. C.; Seinfeld, J. H. Effect of NO_x level on secondary organic aerosol (SOA) formation from the photooxidation of terpenes. *Atmos. Chem. Phys.* **2007**, *7*, 5159−5174.
(11) Hildebrandt, L.; Donahue, N. M.; Pandis, S. N. High formation of secondary organic aerosol from the photo-oxidation of toluene. *Atmos. Chem. Phys.* **2009**, *9*, 2973−2986.
(12) De Gouw, J. A.; et al. Organic Aerosol Formation Downwind from the Deepwater Horizon Oil Spill. *Science* **2011**, *331*, 1295−1299.
(13) Bahreini, R.; et al. Mass spectral analysis of organic aerosols formed downwind of the Deepwater Horizon oil spill. *Environ. Sci. Technol.* **2012**, Submitted.
(14) Ziemann, P. J. Effects of molecular structure on the chemistry of aerosol formation from the OH-radical-initiated oxidation of alkanes and alkenes. *Int. Rev. Phys. Chem.* **2011**, *30*, 161−195.
(15) Kang, E.; Root, M. J.; Brune, W. H. Introducing the concept of Potential Aerosol Mass (PAM). *Atmos. Chem. Phys. Discuss.* **2007**, *7*, 5727−5744.
(16) Lambe, A. T.; Ahern, A. T.; Williams, L. R.; Slowik, J. G.; Wong, J. P. S.; Abbatt, J. P. D.; Brune, W. H.; Ng, N. L.; Wright, J. P.; Croasdale, D. R.; Worsnop, D. R.; Davidovits, P.; Onasch, T. B. Characterization of aerosol photooxidation flow reactors: Heterogeneous oxidation, secondary organic aerosol formation and cloud condensation nuclei activity measurements. *Atmos. Meas. Tech.* **2011**, *4*, 445−461.
(17) McKinley, J. Permeation Tubes: A Simple Path To Very Complex Gas Mixtures. *Gases Instrum.* **2008**, 22−26.
(18) Mao, D.; Weghe, H. V. D.; Lookman, R.; Vanermen, G.; Brucker, N. D.; Diels, L. Resolving the unresolved complex mixture in motor oils using high-performance liquid chromatography followed by comprehensive two-dimensional gas chromatography. *Fuel* **2009**, *88*, 312−318.
(19) Mao, J.; Ren, X.; Brune, W. H.; Olson, J. R.; Crawford, J. H.; Fried, A.; Huey, L. G.; Cohen, R. C.; Heikes, B.; Singh, H. B. Airborne measurement of OH reactivity during INTEX-B. *Atmos. Chem. Phys.* **2009**, *9*, 163−173.
(20) Renbaum, L. H.; Smith, G. D. Artifacts in measuring aerosol uptake kinetics: the roles of time, concentration and adsorption. *Atmos. Chem. Phys.* **2011**, *11*, 6881−6893.
(21) Yaws, C. L.; Yang, H. C. To estimate vapor pressure easily. Antoine coefficients relate vapor pressure to temperature for almost 700 major organic compounds. *Hydrocarbon Process.* **1989**, *68*, 65−68.
(22) Wintenberger, E. Vapor Pressure in JP-10. www.galcit.caltech.edu/EDL/projects/pde/JP10web.xls.
(23) Pierce, J. R.; Engelhart, G. J.; Hildebrandt, L.; Weitkamp, E. A.; Pathak, R. K.; Donahue, N. M.; Robinson, A. L.; Adams, P. J.; Pandis, S. N. Constraining Particle Evolution from Wall Losses, Coagulation, and Condensation-Evaporation in Smog-Chamber Experiments: Optimal Estimation Based on Size Distribution Measurements. *Aerosol Sci. Technol.* **2008**, *42*, 1001−1015.
(24) DeCarlo, P. F.; Kimmel, J. R.; Trimborn, A.; Northway, M. J.; Jayne, J. T.; Aiken, A. C.; Gonin, M.; Fuhrer, K.; Horvath, T.; Docherty, K. S.; Worsnop, D. R.; Jimenez, J. L. Field-Deployable, High-Resolution, Time-of-Flight Aerosol Mass Spectrometer. *Anal. Chem.* **2006**, *78*, 8281−8289.
(25) Sueper, D. T. ToF-AMS Software Downloads. http://cires.colorado.edu/jimenez-group/ToFAMSResources/ToFSoftware .
(26) Aiken, A. C.; et al. O/C and OM/OC ratios of primary, secondary, and ambient organic aerosols with high-resolution time-of-flight aerosol mass spectrometry. *Environ. Sci. Technol.* **2008**, *42*, 4478−4485.
(27) Zhang, Q.; Alfarra, M. R.; Worsnop, D. R.; Allan, J. D.; Coe, H.; Canagaratna, M. R.; Jimenez, J. L. Deconvolution and quantification of hydrocarbon-like and oxygenated organic aerosols based on aerosol mass spectrometry. *Environ. Sci. Technol.* **2005**, *39*, 4938−4952.
(28) Ng, N. L.; Canagaratna, M. R.; Jimenez, J. L.; Zhang, Q.; Ulbrich, I. M.; Worsnop, D. R. Real-Time Methods for Estimating Organic Component Mass Concentrations from Aerosol Mass Spectrometer Data. *Environ. Sci. Technol.* **2011**, *45*, 910−916.
(29) Zhang, Q.; et al. Ubiquity and dominance of oxygenated species in organic aerosols in anthropogenically-influenced Northern Hemisphere midlatitudes. *Geophys. Res. Lett.* **2007**, *34*, L13801.
(30) Docherty, K. S.; Stone, E. A.; Ulbrich, I. M.; DeCarlo, P. F.; Snyder, D. C.; Schauer, J. J.; Peltier, R. E.; Weber, R. J.; Murphy, S. M.; Seinfeld, J. H.; Grover, B. D.; Eatough, D. J.; Jimenez, J. L. Apportionment of primary and secondary organic aerosols in Southern California during the 2005 Study of Organic Aerosols in Riverside (SOAR-1). *Environ. Sci. Technol.* **2008**, *42*, 7655−7662.
(31) Lambe, A. T.; Onasch, T. B.; Massoli, P.; Croasdale, D. R.; Wright, J. P.; Ahern, A. T.; Williams, L. R.; Worsnop, D. R.; Brune, W. H.; Davidovits, P. Laboratory studies of the chemical composition and cloud condensation nuclei (CCN) activity of secondary organic aerosol (SOA) and oxidized primary organic aerosol (OPOA). *Atmos. Chem. Phys.* **2011**, *11*, 8913−8928.
(32) Robinson, A. L.; Donahue, N. M.; Shrivastava, M. K.; Weitkamp, E. A.; Sage, A. M.; Grieshop, A. P.; Lane, T. E.; Pierce, J. R.; Pandis, S. N. Rethinking Organic Aerosols: Semivolatile Emissions and Photochemical Aging. *Science* **2007**, *315*, 1259−1262.
(33) Miracolo, M. A.; Presto, A. A.; Lambe, A. T.; Hennigan, C. J.; Donahue, N. M.; Kroll, J. H.; Worsnop, D. R.; Robinson, A. L. Photo-Oxidation of Low-Volatility Organics Found in Motor Vehicle Emissions: Production and Chemical Evolution of Organic Aerosol Mass. *Environ. Sci. Technol.* **2010**, *44*, 1638−1643.
(34) Miracolo, M. A.; Hennigan, C. J.; Ranjan, M.; Nguyen, N. T.; Gordon, T. D.; Lipsky, E. M.; Presto, A. A.; Donahue, N. M.; Robinson, A. L. Secondary aerosol formation from photochemical aging of aircraft exhaust in a smog chamber. *Atmos. Chem. Phys.* **2011**, *11*, 4135−4147.
(35) Kroll, J. H.; Smith, J. D.; Worsnop, D. R.; Wilson, K. R. Characterization of lightly oxidized organic aerosol formed from the photochemical aging of diesel exhaust particles. *Environ. Chem.* **2012**, Just Accepted.
(36) DeCarlo, P. F.; Dunlea, E. J.; Kimmel, J. R.; Aiken, A. C.; Sueper, D.; Crounse, J.; Wennberg, P. O.; Emmons, L.; Shinozuka, Y.; Clarke, A. Fast airborne aerosol size and chemistry measurements with

the high resolution aerosol mass spectrometer during the MILAGRO Campaign. *Atmos. Chem. Phys.* **2008**, *8*, 4027−4048.
(37) Jimenez, J. L.; et al. Evolution of Organic Aerosols in the Atmosphere. *Science* **2009**, *326*, 1525−1529.
(38) Odum, J. R.; Hoffmann, T.; Bowman, F.; Collins, D.; Flagan, R. C.; Seinfeld, J. H. Gas/particle partitioning and secondary organic aerosol yields. *Environ. Sci. Technol.* **1996**, *30*, 2580−2585.
(39) Donahue, N. M.; Robinson, A. L.; Stanier, C. O.; Pandis, S. N. Coupled partitioning, dilution, and chemical aging of semivolatile organics. *Environ. Sci. Technol.* **2006**, *40*, 2635−2643.
(40) DeCarlo, P. F.; Ulbrich, I. M.; Crounse, J.; Foy, B. D.; Dunlea, E. J.; Aiken, A. C.; Knapp, D.; Weinheimer, A. J.; Campos, T.; Wennberg, P. O.; Jimenez, J. L. Investigation of the sources and processing of organic aerosol over the Central Mexican Plateau from aircraft measurements during MILAGRO. *Atmos. Chem. Phys.* **2010**, *10*, 5257−5280.
(41) Dzepina, K.; Cappa, C.; Volkamer, R.; Madronich, S.; Decarlo, P.; Zaveri, R.; Jimenez, J. Modeling the multiday evolution and aging of secondary organic aerosol during MILAGRO 2006. *Environ. Sci. Technol.* **2011**, *45*, 3496−3503.
(42) Dusanter, S.; Vimal, D.; Stevens, P. S.; Volkamer, R.; Molina, L. T. Measurements of OH and HO_2 concentrations during the MCMA-2006 field campaign−Part 1: Deployment of the Indiana University laser-induced fluorescence instrument. *Atmos. Chem. Phys* **2009**, *9*, 1665−1685.
(43) Hao, L. Q.; et al. Mass yields of secondary organic aerosols from the oxidation of α-pinene and real plant emissions. *Atmos. Chem. Phys.* **2011**, *11*, 1367−1378.
(44) Kroll, J. H.; Smith, J. D.; Che, D. L.; Kessler, S. H.; Worsnop, D. R.; Wilson, K. R. Measurement of fragmentation and functionalization pathways in the heterogeneous oxidation of oxidized organic aerosol. *Phys. Chem. Chem. Phys.* **2009**, *11*, 8005.
(45) Chacon-Madrid, H. J.; Donahue, N. M. Fragmentation vs. functionalization: chemical aging and organic aerosol formation. *Atmos. Chem. Phys.* **2011**, *11*, 10553−10563.
(46) Wilson, K.; Smith, J.; Kessler, S.; Kroll, J. The statistical evolution of multiple generations of oxidation products in the photochemical aging of chemically reduced organic aerosol. *Phys. Chem. Chem. Phys.* **2012**, *14*, 1468−1479.
(47) Ng, N. L.; et al. Organic aerosol components observed in Northern Hemispheric datasets from Aerosol Mass Spectrometry. *Atmos. Chem. Phys.* **2010**, *10*, 4625−4641.
(48) Kroll, J. H.; Donahue, N. M.; Jimenez, J. L.; Kessler, S. H.; Canagaratna, M. R.; Wilson, K. R.; Altieri, K. E.; Mazzoleni, L. R.; Wozniak, A. S.; Bluhm, H.; Mysak, E. R.; Smith, J. D.; Kolb, C. E.; Worsnop, D. R. Carbon oxidation state as a metric for describing the chemistry of atmospheric organic aerosol. *Nat. Chem.* **2011**, *3*, 133−139.
(49) Heald, C. L.; Kroll, J. H.; Jimenez, J. L.; Docherty, K. S.; Decarlo, P. F.; Aiken, A. C.; Chen, Q.; Martin, S. T.; Farmer, D. K.; Artaxo, P. A simplified description of the evolution of organic aerosol composition in the atmosphere. *Geophys. Res. Lett.* **2010**, *37*, L08803.
(50) Ng, N. L.; Canagaratna, M. R.; Jimenez, J. L.; Chhabra, P. S.; Seinfeld, J. H.; Worsnop, D. R. Changes in organic aerosol composition with aging inferred from aerosol mass spectra. *Atmos. Chem. Phys.* **2011**, *11*, 6465−6474.